

In Vitro Biocompatibility of Piezoelectric $K_{0.5}Na_{0.5}NbO_3$ Thin Films on Platinized Silicon Substrates

Nikolai Helth Gaukås, Quy-Susan Huynh, Anishchal A. Pratap, Mari-Ann Einarsrud, Tor Grande, R. M. Damian Holsinger*, and Julia Glaum*



Cite This: *ACS Appl. Bio Mater.* 2020, 3, 8714–8721



Read Online

ACCESS |



Metrics & More



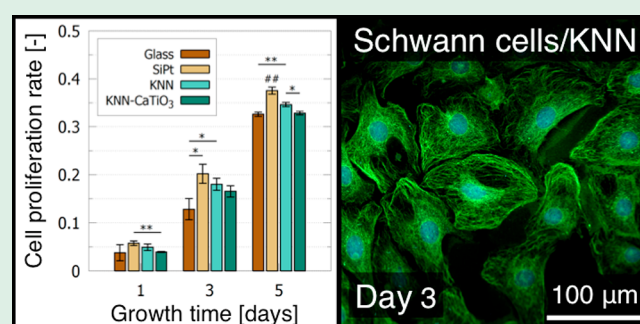
Article Recommendations



Supporting Information

ABSTRACT: Lead-free piezoelectric ceramics like $K_{0.5}Na_{0.5}NbO_3$ (KNN) represent an emerging class of biomaterials for medical technology, as they can be used as components in implantable microelectromechanical systems (MEMS) and bioactive scaffolds for tissue stimulation. Such functional materials can act as working components in future *in vivo* devices, and their addition to current implant designs can greatly improve the biological interaction between host and implant. Despite this, only a few reports have studied the biocompatibility of these materials with living cells. In this work, we investigate the biological response of two different cell lines grown on KNN thin films, and we demonstrate excellent biocompatibility of the KNN films with the cells. Undoped and 0.5 mol % $CaTiO_3$ -doped KNN thin films with nanometer-sized roughness were deposited on platinized silicon (SiPt) substrates, and cell proliferation, viability, and morphology of human 161BR fibroblast cells and rat Schwann cells grown on the KNN films and SiPt substrates were investigated and compared to glass control samples. The results show that proliferation rates for the cells grown on the KNN thin films were equally high or higher than those on the glass control samples, and no cytotoxic effect from either the films or the substrate was observed. The work demonstrates that KNN thin films on SiPt substrates are very promising candidates for components in implantable medical devices.

KEYWORDS: KNN thin films, platinized silicon, topography, wetting, microstructure, cell viability



INTRODUCTION

Piezoelectric ceramics are utilized in a wide range of electromechanical technologies due to their ability to passively transduce electrical and mechanical signals.¹ This characteristic makes them suitable for a wide range of applications, e.g., as transducers for ultrasound imaging, for structural health monitoring of airplanes, or simply as a speaker in a mobile phone. In contrast to electromagnetic systems, piezoelectric components have excellent scaling potential down to the nanometer range, and piezoelectric thin films are therefore of special interest as components in microelectromechanical systems (MEMS).^{2–4} Much research has been devoted to develop processing techniques that allow the integration of piezoelectric films on silicon substrates, which makes them compatible with the wide field of complementary metal–oxide–semiconductor (CMOS) technology.^{4,5}

Piezo- and ferroelectric materials also hold great potential for biomedical applications as they can be utilized as active scaffolds for tissue engineering and energy harvesters, sensors and actuators for implantable microelectronic systems as well as for biosensing and -patterning.^{6–9} Due to the environmental concerns regarding lead-containing piezoceramics like lead zirconate titanate ($Pb(Zr,Ti)O_3$, PZT),¹⁰ lead-free piezo-

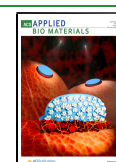
electric thin films have been extensively researched in the last two decades.^{11,12} Among these, ceramic thin films based on potassium sodium niobate ($K_{0.5}Na_{0.5}NbO_3$, KNN) have received much attention due to their good piezoelectric properties and high Curie temperature.^{5,13}

Before introducing such materials to clinical applications, biocompatibility with living tissue needs to be demonstrated. *In vitro* screening assays for cytotoxicity represent as an effective first approximation for biocompatibility.^{14,15} Various forms of KNN ceramics have been subjected to *in vitro* biocompatibility testing, including bulk ceramics,^{16–20} powders and powder extracts^{21,22} as well as films on sapphire and polyethylene terephthalate substrates.^{23,24} In general, KNN ceramics exhibit low acute (24 h)^{19,21–23} and subacute (7 d) toxicity,²⁴ and KNN pellets and films support proliferation and growth of various cell lines on par with controls (e.g.,

Received: September 2, 2020

Accepted: October 28, 2020

Published: November 6, 2020



hydroxyapatite).^{16–20,23} One study has also conducted *in vivo* histological assays of KNN samples in rat thighs and found no sign of inflammation after 7 days of implantation.²³

Here, we report on *in vitro* biocompatibility of KNN thin films on platinized silicon (SiPt) substrates. Undoped and 0.5 mol % CaTiO₃-doped KNN films were synthesized by aqueous chemical solution deposition (CSD) on SiPt substrates based on a previously reported processing route.^{25,26} The biocompatibility of these films was assessed through proliferation, morphology, and viability assays using human 161BR fibroblast cells and rat (glial) Schwann cells. To deconvolute the biological effects from the KNN films and the substrate, SiPt substrates with no deposited film were also tested. Glass coverslips were used as negative controls as they have been reported to support cell attachment and proliferation for both fibroblast^{27,28} and glial cells.^{29,30} The results obtained demonstrate that KNN thin films and SiPt substrates exhibit excellent biocompatibility with both cell lines, and we discuss these findings in the light of bulk and surface properties of the materials.

MATERIALS AND METHODS

Thin Film Synthesis. Undoped KNN (K_{0.5}Na_{0.5}NbO₃) and 0.5 mol % CaTiO₃-doped KNN films (K_{0.4975}Na_{0.4975}Ca_{0.005}Nb_{0.995}Ti_{0.005}O₃, KNN-CaTiO₃) were prepared using aqueous precursor solutions described elsewhere.^{25,26} The solutions were prepared by precipitating niobic acid from an aqueous solution of NH₄NbO(C₂O₄)₂·xH₂O (99.99%, Sigma-Aldrich, St. Louis, MO, U.S.A.) using ammonia solution (25 wt %, VWR Chemicals, Radnor, PA, U.S.A.). The niobic acid precipitate was dissolved in deionized water with DL-malic acid (99%, Sigma-Aldrich) in a molar ratio of 1:2. Dried NaNO₃ (99%, Sigma-Aldrich) and KNO₃ (99%, Alfa Aesar, Haverhill, MA, U.S.A.) were dissolved in the niobium solution using a 5 mol % alkali excess. For KNN-CaTiO₃, Ca²⁺ and Ti⁴⁺ solutions were added to the KNN solution. The Ca²⁺ solution was prepared by dissolving Ca(NO₃)₂·4H₂O (99%, Sigma-Aldrich) in deionized water with ethylenediaminetetraacetic acid (99%, Sigma-Aldrich) in a molar ratio of 1:2. The Ti⁴⁺ solution was prepared by dissolving Ti-isopropoxide (97%, Sigma-Aldrich) in deionized water with citric acid (99%, Sigma-Aldrich) in a molar ratio of 1:3. The pH of the Ca²⁺ and Ti⁴⁺ solutions were adjusted to 8 by using ammonia solution. The pH of the final KNN solutions was adjusted to 7 by addition of ammonia solution.

The surface of platinized silicon (SiPt, 100 nm Pt(111)/30 nm TiO_x/500 nm SiO₂/Si(100), SINTEF MiNaLab, Oslo, Norway) substrates was activated using oxygen plasma cleaning (Femto, Diener Electronics, Ebhausen, Germany), and the KNN solutions were deposited onto the substrates using a spin coater (WS-400A-6NPP/C-1, Laurell Technologies, Montgomery, PA, U.S.A.), operating at 3500 rpm for 40 s. Following deposition, the films were dried on a hot plate at 200 °C for 3 min and pyrolyzed in a rapid thermal processing furnace (AW610, Allwin21, Morgan Hill, CA, U.S.A.) at 550 °C for 5 min in flowing synthetic air using a heating rate of 100 °C min⁻¹. The deposition and heat treatment were repeated 5 times, and the KNN films were postannealed at 700 °C for 5 min in flowing synthetic air using a heating rate of 100 °C min⁻¹. Prior to biological testing the substrate and film samples were sterilized by γ rays using 25 kGy irradiation from a cobalt-60 source at Steritech (Wetherill Park, Sydney, NSW, Australia).

Thin Film Characterization. The phase composition of the films was analyzed by grazing incidence X-ray diffraction (GIXRD) using Cu K α radiation and a 2° incidence angle (D8 Advance, Bruker, Billerica, MA, U.S.A.). Film thickness was determined by scanning electron microscopy (SEM, Ultra 55, Carl Zeiss AG, Oberkochen, Germany) operating at 10 kV acceleration voltage and using an in-lens detector. The surface roughness of the films and the SiPt substrates was studied using atomic force microscopy (AFM,

Multimode V, Veeco Metrology, Plainview, NY, U.S.A.). The hydrophobicity (wettability) of the films and substrate was analyzed by contact angle measurements of deionized water droplets at 37 °C (DSA100, KRÜSS, Hamburg, Germany).

Cell Culture. Human 161BR fibroblast cells were cultured in 3 mL of media (Eagle's MEM with 15% fetal bovine serum (FBS), 2 mM L-glutamine, 1% nonessential amino acids (NEAA), and 1% Penicillin Streptomycin (Pen-Strep)) at 37 °C with 5% CO₂ in a T25 flask until confluent. Rat Schwann cells were cultured in 3 mL of media (Ham's F12 with 10% FBS, 2 mM L-glutamine, and 1% Pen-Strep) at 37 °C with 5% CO₂ in a T25 flask until confluent. All media and components were purchased from Sigma-Aldrich (Seven Hills, NSW, Australia). The media for both cell lines were changed every 3 days. When confluent, the cells were lifted from the T25 flask using 0.025% trypsin (Gibco, Cat no. 15400054 in 1× phosphate buffered saline (PBS) no calcium, no magnesium) and seeded onto glass coverslips (control, Hurst Scientific, WA, Australia), SiPt, KNN/SiPt and KNN-CaTiO₃/SiPt in a 24-well plate along with 500 μ L of media. Three samples were used for each material and control.

Cell Proliferation Assay (MTT). Cell proliferation of 161BR fibroblast and Schwann cells on SiPt substrates and KNN thin films was screened using an MTT colorimetric assay. The cell densities seeded for the proliferation assay were 2.0×10^3 cells per well (161BR fibroblast cells) and 4.3×10^3 cells per well (Schwann cells). The cells were grown in media at 37 °C with 5% CO₂ for 1, 3, 5, and 7 days (triplicates at each point). The media was changed every 2 days after seeding. The colorimetric assay was performed after 1, 3, 5, and 7 days. The culture media was removed, and 50 μ L of an MTT solution (5 mg mL⁻¹ MTT, VWR/Amresco, Cat no. 97062-380 in 1× PBS (1%)) and 450 μ L of serum-free Eagle's MEM (161BR fibroblast cells) or serum-free Ham's F12 medium (Schwann cells) were added to the wells. The 24-well plate was incubated for 4 h at 37 °C with 5% CO₂. Following this, the MTT solution was carefully removed and the formed formazan crystals were dissolved in an MTT solvent (4 mM HCl and 0.1% Nonidet P-40 (VWR/Amresco) in isopropanol). The plate was wrapped in foil and left on a rocker for 10 min. The MTT solvent was then collected and placed into a 96-well plate for spectrophotometric analysis, measuring absorption at 560 nm wavelength (Hidex Chameleon Multilabel plate reader, Turku, Finland). Statistical analysis of the data was performed using one-way ANOVA and statistical significance was set at $p < 0.05$.

Cell Morphology Assay. Cell morphology of 161BR fibroblast cells and Schwann cells on SiPt substrates and KNN thin films was studied using SEM. The cell densities seeded for SEM imaging were 3.9×10^3 cells per well (161BR fibroblast cells) and 6.3×10^3 cells per well (Schwann cells). The cells were grown in media at 37 °C with 5% CO₂ for 5 days (161BR fibroblast cells) and 3 days (Schwann cells). For the 161BR fibroblast cells, the media was changed 2 days after seeding. After 3–5 days, the cells were washed twice with 500 μ L of warm 1× PBS and fixed using 300 μ L glutaraldehyde (3% in 1× PBS, preheated to 37 °C, Sigma-Aldrich). The cells were stored in the plate with glutaraldehyde for 20 h at 4 °C in a zip lock bag to prevent loss of glutaraldehyde through evaporation. The following day, the glutaraldehyde was removed, and the cells were washed twice with 300 μ L of 1× PBS at 4 °C for 10 min. Prior to dehydration, the cells were hydrated twice with deionized water for 10 min. The cells were then gradually dehydrated using single washes of 30, 50, 70, 80, and 90% (v/v) ethanol and two washes with 100% ethanol, with each wash lasting 12 min. Following this, the dehydrated cells were left for 24 h for the ethanol to completely evaporate. The samples were imaged using SEM (TM3030, Hitachi, Tokyo, Japan).

Cell Viability Assay (Immunofluorescence). Cell viability of 161BR fibroblast and Schwann cells on SiPt substrates and KNN thin films was studied using immunofluorescent microscopy. The cell densities seeded for immunofluorescent microscopy were 1.3×10^3 cells per well (161BR fibroblast cells) and 6.3×10^3 cells per well (Schwann cells). The cells were grown in media at 37 °C with 5% CO₂ for 5 days (161BR fibroblast cells) and 3 days (Schwann cells). For the 161BR fibroblast cells, the media was changed 2 days after seeding. When cells reached ~90% confluency (after 3–5 days), the

cells were washed 2 times with 600 μL of 1 \times PBS and fixed using 300 μL of paraformaldehyde (4% (w/v), pH 7.4) warmed to 37 $^{\circ}\text{C}$. The 24-well plate was placed inside a zip lock bag and left in the incubator for 10 min at 37 $^{\circ}\text{C}$ with 5% CO_2 . The paraformaldehyde was removed, and the cells were washed three times with 300 μL of 1 \times PBS. The cells were then permeabilized with 300 μL of Triton X-100 in 1 \times PBS (0.1%) for 15 min at room temperature. Permeabilization facilitates antibody penetration into the cells. Following this, the cells were washed three times with 300 μL of 1 \times PBS. The cells were blocked using 300 μL of bovine serum albumin (BSA) in 1 \times PBS (1%) for 60 min at room temperature to prevent nonspecific antibody–protein interaction. Cells were immunostained with 300 μL of monoclonal β -tubulin primary antibody (1:5000 dilution in PBS, Sigma-Aldrich, Cat no. T7816) which was left in for 16 h at 4 $^{\circ}\text{C}$. The next day, the primary antibody was removed, and the cells were washed three times with 300 μL of 1 \times PBS. The β -tubulin primary antibodies were detected by adding 300 μL of Alexa Fluor 488-conjugated rabbit antihorse IgG (H+L) secondary antibody (1:5000 dilution in PBS, Life Technologies, Cat no. A1005534) for 45 min in room temperature and away from light. Following this, the cells were washed once with 300 μL of 1 \times PBS. In order to stain cell nuclei, 50 μL of 4',6-diamidino-2-phenylindole (DAPI, 0.1 g L^{-1} PBS, Sigma-Aldrich, Cat no. D9542-10MG) was added for 3 min at room temperature. The cells were then washed twice with 300 μL of 1 \times PBS, and glass coverslips were mounted on the samples using dibutyl phthalate in xylene (DPX). The immunostained cells were imaged using confocal microscopy (LSM 800, Carl Zeiss AG).

RESULTS

Microstructure and Phase Composition of the KNN Films and SiPt Substrates. Cross sectional SEM micrographs of the KNN and KNN- CaTiO_3 thin films prepared from CSD on SiPt demonstrate that the KNN films were dense, homogeneous, and without cracks, pinholes, or other macroscopic defects (Figure 1). The thickness of the KNN

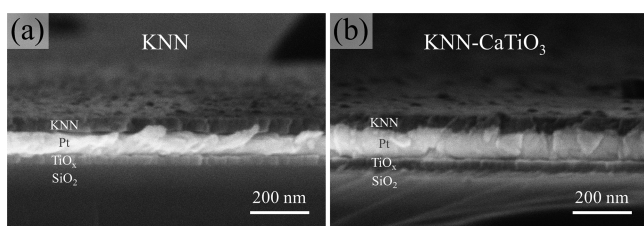


Figure 1. Cross sectional SEM micrographs of (a) KNN and (b) KNN- CaTiO_3 thin films on SiPt substrates. The KNN films and the different layers of the substrate are indicated on the micrographs.

films fabricated from 6 depositions was ~ 50 nm for both compositions. GIXRD patterns of the KNN and KNN- CaTiO_3 thin films are presented in Figure S1 in the Supporting Information. All of the Bragg reflections can be assigned to monoclinic $\text{K}_{0.5}\text{Na}_{0.5}\text{NbO}_3$ ³¹ and the substrate, confirming that single phase KNN was deposited on SiPt substrates using the aqueous CSD route.^{25,26}

The surface morphologies of the glass coverslips, SiPt substrates, and the KNN and KNN- CaTiO_3 thin films are presented in Figure 2. The topography observed on the two KNN samples originates from the grain structure of the KNN films. The average grain size is ~ 50 and ~ 45 nm for the KNN and KNN- CaTiO_3 thin films, respectively. The surface topography of the glass coverslips and SiPt substrates is significantly smoother than for the films. The root-mean-square (RMS) surface roughness (S_q), plotted in Figure 2e, was calculated for each sample based on 25 μm^2 scans at the

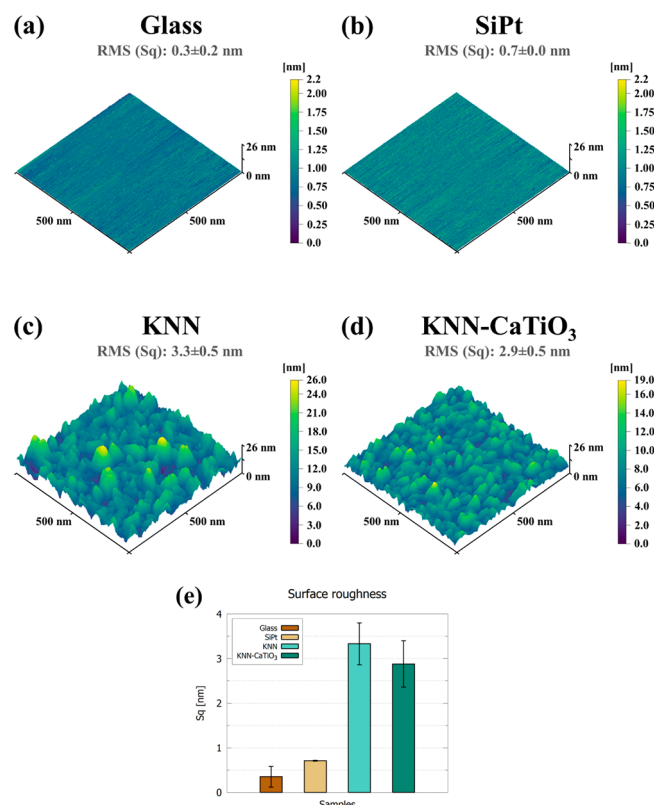


Figure 2. AFM topography images of (a) glass coverslips, (b) SiPt substrates, (c) KNN thin films, and (d) KNN- CaTiO_3 thin films. The ranges of the scalebars in panels a–d differ. (e) The RMS roughness of the samples calculated from AFM measurements.

center and edge of the samples. The surface topographies of the samples are reflected in the S_q values.

The contact angles of water droplets at 37 $^{\circ}\text{C}$ on SiPt substrates, KNN thin films and KNN- CaTiO_3 thin films as well as glass coverslips are presented in Figure 3. All samples show hydrophilic surfaces without significant difference between the materials.

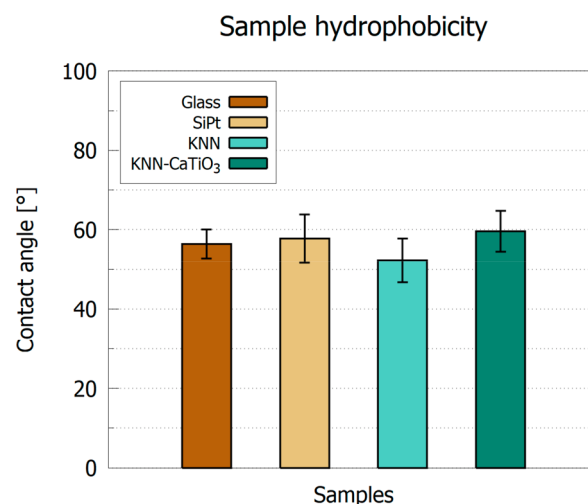


Figure 3. Contact angles of distilled water drops on top of the samples at 37 $^{\circ}\text{C}$. The values are averages from measurements on 10 drops.

Biocompatibility. Cell proliferation rates after 1, 3, 5, and 7 days for 161BR fibroblast and Schwann cells grown on SiPt substrates, KNN thin films, KNN-CaTiO₃ thin films, and glass coverslips (control) are shown in Figure 4a,b, respectively.

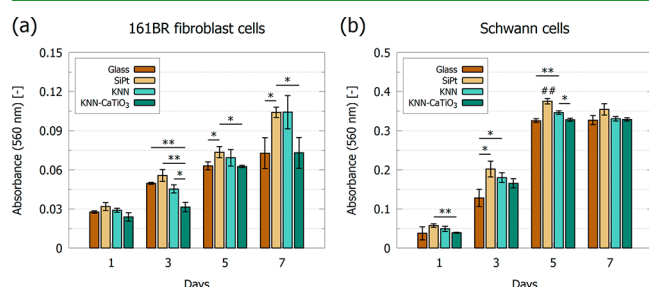


Figure 4. Proliferation rates of (a) human 161BR fibroblast and (b) rat Schwann cells after being grown for 1, 3, 5, and 7 days on glass coverslips (control), SiPt substrates, KNN thin films and KNN-CaTiO₃ thin films. Statistical significance is indicated (* = $p < 0.05$, ** = $p < 0.01$). ## refers to a difference of $p < 0.01$ between SiPt and each of the other samples.

Proliferation of 161BR fibroblast cells is highest on the SiPt substrates at most time points, while a statistical difference between the glass control, KNN, and KNN-CaTiO₃ thin films was often not observed. After 5 days, the proliferation of Schwann cells is highest on the SiPt substrates followed by that on the KNN thin films, whereas proliferation rates on the KNN-CaTiO₃ thin films is equal to the control. The lack of change in proliferation from day 5 to 7 for the Schwann cells is due to cells reaching confluency/overcrowding in the sample wells.

Cell morphology and viability of 161BR fibroblast and Schwann cells after being grown on SiPt substrates, KNN thin films and KNN-CaTiO₃ thin films are displayed in Figure 5.

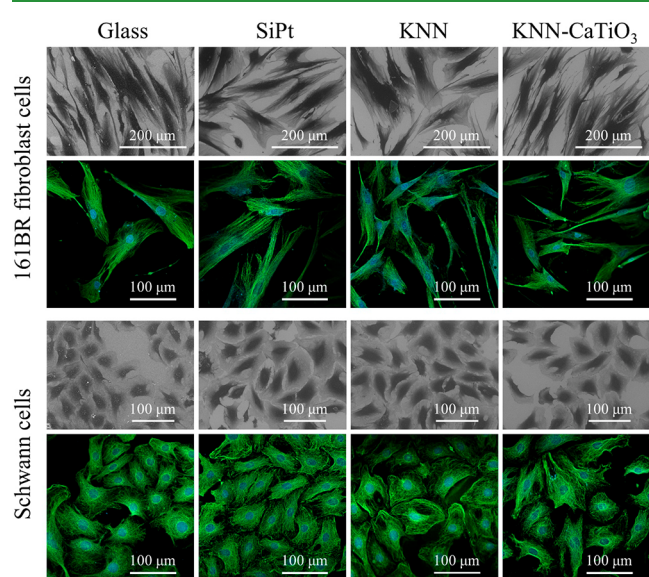


Figure 5. SEM micrographs and confocal immunofluorescence images of 161BR fibroblast cells (top two rows) and Schwann cells (bottom two rows) after being grown on glass coverslips, SiPt substrates, KNN thin films and KNN-CaTiO₃ thin films for 5 (161BR fibroblast cells) and 3 days (Schwann cells). Cell cytoskeletons and nuclei are stained with β -tubulin (green) and DAPI (blue), respectively.

Both cell lines adhered well to all of the materials tested. The 161BR fibroblast cells were observed to spread out more on the SiPt substrates and the KNN thin films compared to the cells grown on the control and the KNN-CaTiO₃ thin films. A higher density of Schwann cells was observed growing on the SiPt substrates and the KNN thin films compared to the growth of cells on the control and the KNN-CaTiO₃ thin films.

DISCUSSION

The variations in viability and proliferation rate of cells grown on different materials can be attributed to surface properties (e.g., topography, hydrophobicity, and surface charges) and/or to bulk properties (e.g., ion release and stiffness) of the substrate materials. In this study we assessed the biocompatibility properties of various sample types *in vitro* to determine their suitability for incorporation into biomedical devices.

Surface Properties. Surface topography can facilitate cell orientation/adhesion, morphology, differentiation and proliferation.^{32–34} Manipulation of cell alignment and growth using micrometer-sized topography has been demonstrated for fibroblast³⁵ and glial cells.³⁶ Nanometer-sized topography, however, indirectly affects cell behavior by influencing protein adsorption and by resembling the natural extracellular matrix.³⁷ Different proteins have differing affinities for size and shape of surface topographic features, and the reported effects vary. Nanometer-sized topography has been demonstrated to influence fibroblast cells with cell proliferation and spreading increasing with decreasing surface roughness in the ranges of 23–0.7 nm³⁸ and 95–13 nm.³⁹ The research on glial cells is more nuanced, and these cells have been found to be unaffected by nanotopography in the range of 0.7–23 nm.³⁸ Instead, they seem to prefer “grassy” regions with structures of height 230 nm and diameter of 60 nm over smoother regions with imprints of 115 nm depth and 100–250 nm width.⁴⁰ In the present study, the average surface roughness (S_q) of the KNN (3.3 ± 0.5 nm) and KNN-CaTiO₃ films (2.9 ± 0.5 nm) was found to be greater than the roughness of the SiPt substrates (0.7 ± 0.1 nm) and glass coverslips (0.3 ± 0.2 nm). This difference between the coated and uncoated substrates is related to the growth of grains in the ceramic films during heat treatment. The slightly larger roughness of the KNN compared to the KNN-CaTiO₃ films is caused by a larger average grain size in undoped KNN as reported previously.²⁶ The roughness of the samples in the present study does not appear to influence cell behavior, as cells proliferated and spread equally well on the glass controls, SiPt substrates and the KNN films (Figures 4 and 5). Compared to other studies, these results demonstrate that the surface topography differences in our work (0.3–3.3 nm) are too small to influence the behavior of fibroblast and glial cells. Glial cells have been reported to be unaffected by nanosized differences in the range of 0.7–23 nm,³⁸ and our results suggests that there is also a lower limit for fibroblast cells, where differences in the surface roughness do not influence cell behavior.

Surface hydrophobicity of biomaterials is directly linked to biocompatibility since the proteins forming binding sites for cells (e.g., fibrin and albumin) adhere to the biomaterial using hydrophobic domains.^{32,41} However, a surface that is too hydrophobic will cause protein relaxation and loss of biological activity. The composition and orientation of proteins binding to the surface is governed by the surface hydrophobicity, and different cell lines have different preferences regarding protein binding sites. Fibroblast cells have been reported to have their

peak proliferation rate on surfaces with contact angles (θ_c) around 60–70°. ^{42–44} The case is not so clear for glial cells, and increased proliferation has been observed for both hydrophobic over hydrophilic surfaces ⁴⁵ as well as hydrophilic over hydrophobic surfaces. ^{46,47} The surface hydrophobicity measurement in this work demonstrates that all of the samples are moderately hydrophilic with contact angles between 50° and 60° (Figure 4). These values are in agreement with literature on other ceramics and metals. ⁴⁸ The observed differences in surface hydrophobicity between the samples in this study are minor and do not seem to have a significant impact on cell behavior. However, overall, cell adhesion, viability and proliferation of both cell lines were good, suggesting that a surface hydrophobicity of 50–60° is suitable for growth of both fibroblast and glial cells. This is in agreement with previous studies on fibroblast cells ^{42–44} and suggests that glial cells are compatible with moderately hydrophilic surfaces in addition to more extreme wetting angles. ^{45–47} The wetting behavior in an *in vivo* scenario, however, might vary, as this characteristic is quite sensitive to many factors such as changes in topography or physicochemical conditions. ⁴⁹

Electric surface potentials on poled KNN ceramics have been shown to promote higher cell proliferation rates compared to unpoled KNN ceramics. ^{16,18–20} The strength of this surface polarization has been reported to correlate positively with cell proliferation, ²⁰ but the optimal direction of polarization for cell growth seems to vary between cell lines. ^{18,19} A macroscopic polarization of ferroelectric samples can be obtained by electrical poling and KNN has been reported to retain most of the ferroelectric functionality after γ ray-sterilization up to 3000 kGy. ⁵⁰ The KNN films in this study were not electrically poled before cell testing and should therefore exhibit a random ferroelectric domain distribution. Even though the material is in its polar state and a polarization state can be assigned to each domain, the sum of all domain contributions to the macroscopic polarization cancels out due to the random orientation of the domains. The ferroelectric domains of the unpoled films are limited to the sizes of the grains (<100 nm) and are thus expected to be too small to influence cell behavior. The effect of both poling and mechanical stimulation of the KNN samples is an interesting approach that should be considered in future studies evaluating the biocompatibility of these materials.

Bulk properties. The leaching of ions, molecules or particles from a material can be harmful to cells if the material releases products that are toxic. Release processes from a bulk material can be slow, and observing the chronic cytotoxic effect of materials in short-term studies is usually impossible. ^{51,52} This has been exemplified with Pb(Zr,Ti)O₃-based ceramics that seemingly show no cytotoxicity *in vitro* and *in vivo* in short-term experiments. ²³ In contrast to that, leaching studies performed on powders show higher release rates due to their higher surface area, providing a better indicator for long-term toxicity effects. In the present study, several different materials have been brought in contact with cells. The SiPt substrates, mostly comprised of Si and platinum metal, are expected to be chemically inert in the cell culture medium and to not release ions during *in vitro* studies. For KNN, ion release assays have been performed on powders in several studies. ^{21–23,53} The release of K⁺ and Na⁺ is 1–2 orders of magnitude higher than that of Nb⁵⁺ due to the lower ionic strength of these ions. For 0.5 wt % powder suspensions in distilled water at room temperature the K⁺/Na⁺ release is 1–3 mmol L⁻¹. ⁵³ These

values are not negligible, and studies have linked the release of ions from KNN powders to a reduction in the rate of proliferation. ^{21,22} Although all cations in KNN (including Ca²⁺ and Ti⁴⁺ in the doped KNN composition in this work) are nontoxic in small concentrations, ^{10,54,55} local concentrations of leached ions can be high. Leaching of Na⁺ and K⁺ from soda-lime glass in water has been reported. ⁵⁶ Assuming the release of alkali metals is the cause of differences observed in the cell experiments, the SiPt samples should show the best performance, which is indeed the case for most of the time points investigated in both cell line experiments (Figure 4), whereas the alkali-containing samples perform mostly on par with one another.

Material stiffness has been demonstrated to influence cell adhesion, spreading, proliferation, and differentiation. ^{57,58} Most reports have studied the effect of substrate stiffness in the range of 10¹–10⁶ Pa. In general, increased substrate stiffness is associated with enhanced adhesion, enlarged cell spreading and higher proliferation rates. Glial cells fail to grow on substrates with stiffnesses in the range 10²–10³ Pa but overrun the glass control samples (>10 GPa) in the same experiment. ⁵⁹ However, not all cell types show a monotonic dependence on substrate stiffness. Fibroblast cells exhibit increased proliferation and spreading with increasing substrate stiffness in the range from 100 Pa to 100 kPa, but they also start to produce stress fibers above 10 kPa. ⁶⁰ Yet, fibroblast cells have been reported to proliferate well on glass substrates. ^{27,28} The bulk Young's moduli of the materials used in the current study are reported to be in the range of 80–170 GPa, ^{61–63} while for KNN films on SiPt, values between 70 and 100 GPa can be found. ⁶⁴ These values are much higher than the values typically used when studying the effect of substrate stiffness on cells and it is not clear from the literature whether the differences in such a high stiffness regime will influence cell behavior. Moreover, the three Si-based samples in this study (SiPt, KNN/SiPt, and KNN-CaTiO₃/SiPt) and especially the two KNN films should have almost identical stiffnesses, as the mechanical characteristics of the film is expected to be dominated by the properties of the substrate. This suggests that the differences observed between these samples in the *in vitro* assays are not caused by the materials' stiffness.

CONCLUSION

The *in vitro* biocompatibility of KNN films was investigated using human 161BR fibroblast and rat Schwann cells. Undoped and 0.5 mol % CaTiO₃-doped KNN thin films were deposited on SiPt substrates by aqueous CSD and the proliferation, morphology and viability of cells grown on the films were assessed. Both KNN film compositions support cell attachment, spreading and proliferation equally well or better than the glass control samples. The results further suggest that fibroblast and glial cells are indifferent to differences in surface roughness between 0.3 and 3.3 nm and that these cell types respond well to moderately hydrophilic surfaces ($\theta_c \approx 50$ –60°). When evaluated together with previous work on biocompatibility of KNN ceramics, our findings strongly support the description of KNN as a noncytotoxic ceramic that exhibits biocompatibility with a wide range of cell lines. To the best of our knowledge, our results are the first to establish platinized silicon substrates as noncytotoxic. This work demonstrates that KNN thin films and SiPt substrates exhibit excellent *in vitro* biocompatibility and that KNN films

hold the potential as functional components in implantable medical devices.

■ ASSOCIATED CONTENT


SI Supporting Information


The Supporting Information is available free of charge at <https://pubs.acs.org/doi/10.1021/acsabm.0c01111>.

XRD patterns of KNN films (PDF)

■ AUTHOR INFORMATION

Corresponding Authors

Julia Glaum – Department of Materials Science and Engineering, NTNU Norwegian University of Science and Technology, Trondheim, Norway;  orcid.org/0000-0002-4871-4438; Email: julia.glaum@ntnu.no


R. M. Damian Holsinger – Laboratory of Molecular Neuroscience and Dementia, Brain and Mind Centre, Faculty of Medicine and Health and Discipline of Pathology, School of Medical Sciences, Faculty of Medicine and Health, The University of Sydney, Camperdown, NSW 2050, Australia;  orcid.org/0000-0002-4447-0835; Email: damian.holsinger@sydney.edu.au

Authors

Nikolai Helth Gaukås – Department of Materials Science and Engineering, NTNU Norwegian University of Science and Technology, Trondheim, Norway; Laboratory of Molecular Neuroscience and Dementia, Brain and Mind Centre, Faculty of Medicine and Health, The University of Sydney, Camperdown, NSW 2050, Australia

Quy-Susan Huynh – Laboratory of Molecular Neuroscience and Dementia, Brain and Mind Centre, Faculty of Medicine and Health and Discipline of Pathology, School of Medical Sciences, Faculty of Medicine and Health, The University of Sydney, Camperdown, NSW 2050, Australia

Anishchal A. Pratap – Laboratory of Molecular Neuroscience and Dementia, Brain and Mind Centre, Faculty of Medicine and Health and Discipline of Pathology, School of Medical Sciences, Faculty of Medicine and Health, The University of Sydney, Camperdown, NSW 2050, Australia

Mari-Ann Einarsrud – Department of Materials Science and Engineering, NTNU Norwegian University of Science and Technology, Trondheim, Norway;  orcid.org/0000-0002-3017-1156

Tor Grande – Department of Materials Science and Engineering, NTNU Norwegian University of Science and Technology, Trondheim, Norway

Complete contact information is available at: <https://pubs.acs.org/doi/10.1021/acsabm.0c01111>

Author Contributions

N.H.G., Q.S.H., R.M.D.H., and J.G. conceived and designed the experiments. N.H.G. synthesized the thin films and performed SEM and XRD on the thin films. N.H.G. and Q.S.H. cultured cells, performed the proliferation assays, and imaged the cells with SEM. N.H.G., Q.S.H., and A.A.P. stained the cells. A.A.P. imaged the cells with confocal microscope. All authors analyzed the data. The manuscript was written through contributions of all authors. All authors have given approval to the final version of the manuscript.

Notes

The authors declare no competing financial interest.

■ ACKNOWLEDGMENTS

Financial support from the Research Council of Norway through the NANO2021 project PIEZOMED Project No. 250184 and the FRIPRO Project 250098 are acknowledged. The Research Council of Norway is acknowledged for the support to the Norwegian Microand Nano-Fabrication Facility, NorFab, Project No. 245963/F50. We acknowledge Ph.D. candidate Viviann Hole for performing the AFM measurements and Johannes Ofstad for performing the contact angle measurements. Dr. Philip Boughton is acknowledged for general discussions and support with sample sterilization.

■ REFERENCES

- (1) Manjón-Sanz, A. M.; Dolgos, M. R. Applications of Piezoelectrics: Old and New. *Chem. Mater.* **2018**, *30* (24), 8718–8726.
- (2) Damjanovic, D. Ferroelectric, Dielectric and Piezoelectric Properties of Ferroelectric Thin Films and Ceramics. *Rep. Prog. Phys.* **1998**, *61*, 1267.
- (3) Trolhier-Mckinstry, S.; Murali, P. Thin Film Piezoelectrics for MEMS. *J. Electroceram.* **2004**, *12* (1–2), 7–17.
- (4) Murali, P.; Polcawich, R. G.; Trolhier-Mckinstry, S. Piezoelectric Thin Films for Sensors, Actuators, and Energy Harvesting. *MRS Bull.* **2009**, *34* (9), 658–664.
- (5) Zhang, S. W.; Zhou, Z.; Luo, J.; Li, J. F. Potassium-Sodium-Niobate-Based Thin Films: Lead Free for Micro-Piezoelectrics. *Ann. Phys.* **2019**, *531* (7), 1800525.
- (6) Salim, M.; Salim, D.; Chandran, D.; Aljibori, H. S.; Kherbeet, A. S. Review of Nano Piezoelectric Devices in Biomedicine Applications. *J. Intell. Mater. Syst. Struct.* **2018**, *29* (10), 2105–2121.
- (7) Blázquez-Castro, A.; García-Cabañes, A.; Carrascosa, M. Biological Applications of Ferroelectric Materials. *Appl. Phys. Rev.* **2018**, *5*, 041101.
- (8) Fu, Y. Q.; Luo, J. K.; Nguyen, N. T.; Walton, A. J.; Flewitt, A. J.; Zu, X. T.; Li, Y.; McHale, G.; Matthews, A.; Iborra, E.; Du, H.; Milne, W. I. Advances in Piezoelectric Thin Films for Acoustic Biosensors, Acoustofluidics and Lab-on-Chip Applications. *Prog. Mater. Sci.* **2017**, *89*, 31–91.
- (9) Chorsi, M. T.; Curry, E. J.; Chorsi, H. T.; Das, R.; Baroody, J.; Purohit, P. K.; Ilies, H.; Nguyen, T. D. Piezoelectric Biomaterials for Sensors and Actuators. *Adv. Mater.* **2019**, *31*, 1802084.
- (10) Rödel, J.; Jo, W.; Seifert, K. T. P.; Anton, E. M.; Granzow, T.; Damjanovic, D. Perspective on the Development of Lead-Free Piezoceramics. *J. Am. Ceram. Soc.* **2009**, *92* (6), 1153–1177.
- (11) Safari, A.; Abazari, M. Lead-Free Piezoelectric Ceramics and Thin Films. *IEEE Trans. Ultrason. Ferroelectr. Freq. Control* **2010**, *57* (10), 2165–2176.
- (12) Malic, B.; Kupec, A.; Vojisavljevic, K.; Pecnik, T. Lead-Free Ferroelectric Thin Films. In *Handbook of Sol-Gel Science and Technology*; Klein, L., Aparicio, M., Jitianu, A., Eds.; Springer International Publishing: Berlin, 2016; pp 1–28.
- (13) Seog, H. J.; Ullah, A.; Ahn, C. W.; Kim, I. W.; Lee, S. Y.; Park, J.; Lee, H. J.; Won, S. S.; Kim, S.-H. Recent Progress in Potassium Sodium Niobate Lead-Free Thin Films. *J. Korean Phys. Soc.* **2018**, *72* (12), 1467–1483.
- (14) Bruinink, A.; Luginbuehl, R. Evaluation of Biocompatibility Using In Vitro Methods: Interpretation and Limitations. In *Tissue Engineering III: Cell - Surface Interactions for Tissue Culture*; Springer: Berlin, 2011; pp 117–152.
- (15) Aslantürk, Ö. S. In Vitro Cytotoxicity and Cell Viability Assays: Principles, Advantages, and Disadvantages. In *Genotoxicity: A Predictable Risk to Our Actual World*; Larramendy, M., Soloneski, S., Eds.; IntechOpen, 2018; pp 1–18.
- (16) Wang, Q.; Yang, J.; Zhang, W.; Khoie, R.; Li, Y. M.; Zhu, J. G.; Chen, Z. Q. Manufacture and Cytotoxicity of a Lead-Free Piezoelectric Ceramic as a Bone Substitute-Consolidation of Porous Lithium Sodium Potassium Niobate by Cold Isostatic Pressing. *Int. J. Oral Sci.* **2009**, *1* (2), 99–104.

- (17) Dubey, A. K.; Kakimoto, K.; Obata, A.; Kasuga, T. Enhanced Polarization of Hydroxyapatite Using the Design Concept of Functionally Graded Materials with Sodium Potassium Niobate. *RSC Adv.* **2014**, *4* (47), 24601–24611.
- (18) Tan, G.; Wang, S.; Zhu, Y.; Zhou, L.; Yu, P.; Wang, X.; He, T.; Chen, J.; Mao, C.; Ning, C. Surface-Selective Preferential Production of Reactive Oxygen Species on Piezoelectric Ceramics for Bacterial Killing. *ACS Appl. Mater. Interfaces* **2016**, *8* (37), 24306–24309.
- (19) Chen, W.; Yu, Z.; Pang, J.; Yu, P.; Tan, G.; Ning, C. Fabrication of Biocompatible Potassium Sodium Niobate Piezoelectric Ceramic as an Electroactive Implant. *Materials* **2017**, *10*, 345.
- (20) Yao, T.; Chen, J.; Wang, Z.; Zhai, J.; Li, Y.; Xing, J.; Hu, S.; Tan, G.; Qi, S.; Chang, Y.; Yu, P.; Ning, C. The Antibacterial Effect of Potassium-Sodium Niobate Ceramics Based on Controlling Piezoelectric Properties. *Colloids Surf., B* **2019**, *175*, 463–468.
- (21) Yu, S.-W.; Kuo, S.-T.; Tuan, W.-H.; Tsai, Y.-Y.; Su, C.-H. Ion Release from Three Lead-Free Piezoelectric Ceramics and Their Physical and Cytotoxicity Characteristics. *Mater. Lett.* **2011**, *65* (23–24), 3522–3524.
- (22) Yu, S.; Kuo, S.; Tuan, W.; Tsai, Y.; Wang, S. Cytotoxicity and Degradation Behavior of Potassium Sodium Niobate Piezoelectric Ceramics. *Ceram. Int.* **2012**, *38* (4), 2845–2850.
- (23) Jeong, C. K.; Han, J. H.; Palneedi, H.; Park, H.; Hwang, G.; Joung, B.; Kim, S.; Shin, H. J.; Kang, I.; Ryu, J.; Lee, K. J. Comprehensive Biocompatibility of Nontoxic and High-Output Flexible Energy Harvester Using Lead-Free Piezoceramic Thin Film. *APL Mater.* **2017**, *5*, 074102.
- (24) Kim, B. Y.; Lee, W. H.; Hwang, H. G.; Kim, D. H.; Kim, J. H.; Lee, S. H.; Nahm, S. Resistive Switching Memory Integrated with Nanogenerator for Self-Powered Bioimplantable Devices. *Adv. Funct. Mater.* **2016**, *26* (29), 5211–5221.
- (25) Helth Gaukas, N.; Dale, S. M.; Ræder, T. M.; Toresen, A.; Holmestad, R.; Glaum, J.; Einarsrud, M.-A.; Grande, T. Controlling Phase Purity and Texture of $K_{0.5}Na_{0.5}NbO_3$ Thin Films by Aqueous Chemical Solution Deposition. *Materials* **2019**, *12*, 2042.
- (26) Gaukås, N. H.; Glaum, J.; Einarsrud, M.-A.; Grande, T. Ferroelectric and Dielectric Properties of Ca^{2+} -Doped and Ca^{2+} - Ti^{4+} Co-Doped $K_{0.5}Na_{0.5}NbO_3$ Thin Films. *J. Mater. Chem. C* **2020**, *8*, 5102–5111.
- (27) Saltzman, W. M.; Parsons-Wingerter, P.; Leong, K. W.; Lin, S. Fibroblast and Hepatocyte Behavior on Synthetic Polymer Surfaces. *J. Biomed. Mater. Res.* **1991**, *25* (6), 741–759.
- (28) Marchesano, V.; Gennari, O.; Mecozzi, L.; Grilli, S.; Ferraro, P. Effects of Lithium Niobate Polarization on Cell Adhesion and Morphology. *ACS Appl. Mater. Interfaces* **2015**, *7* (32), 18113–18119.
- (29) Vleggeert-Lankamp, C. L. A. M.; Pêgo, A. P.; Lakke, E. A. J. F.; Deenen, M.; Marani, E.; Thomeer, R. T. W. M. Adhesion and Proliferation of Human Schwann Cells on Adhesive Coatings. *Biomaterials* **2004**, *25* (14), 2741–2751.
- (30) Yuan, Y.; Zhang, P.; Yang, Y.; Wang, X.; Gu, X. The Interaction of Schwann Cells with Chitosan Membranes and Fibers in Vitro. *Biomaterials* **2004**, *25* (18), 4273–4278.
- (31) Tellier, J.; Malic, B.; Dkhil, B.; Jenko, D.; Cilensek, J.; Kosec, M. Crystal Structure and Phase Transitions of Sodium Potassium Niobate Perovskites. *Solid State Sci.* **2009**, *11* (2), 320–324.
- (32) Harvey, A. G.; Hill, E. W.; Bayat, A. Designing Implant Surface Topography for Improved Biocompatibility. *Expert Rev. Med. Devices* **2013**, *10* (2), 257–267.
- (33) Simitzi, C.; Ranella, A.; Stratakis, E. Controlling the Morphology and Outgrowth of Nerve and Neuroglial Cells: The Effect of Surface Topography. *Acta Biomater.* **2017**, *51*, 21–52.
- (34) Nguyen, A. T.; Sathe, S. R.; Yim, E. K. F. From Nano to Micro: Topographical Scale and Its Impact on Cell Adhesion, Morphology and Contact Guidance. *J. Phys.: Condens. Matter* **2016**, *28* (18), 183001.
- (35) Den Braber, E. T.; de Ruijter, J. E.; Smits, H. T. J.; Ginsel, L. A.; von Recum, A. F.; Jansen, J. A. Effect of Parallel Surface Microgrooves and Surface Energy on Cell Growth. *J. Biomed. Mater. Res.* **1995**, *29* (4), 511–518.
- (36) Schmalenberg, K. E.; Uhrich, K. E. Micropatterned Polymer Substrates Control Alignment of Proliferating Schwann Cells to Direct Neuronal Regeneration. *Biomaterials* **2005**, *26* (12), 1423–1430.
- (37) Lord, M. S.; Foss, M.; Besenbacher, F. Influence of Nanoscale Surface Topography on Protein Adsorption and Cellular Response. *Nano Today* **2010**, *5* (1), 66–78.
- (38) Pennisi, C. P.; Sevcencu, C.; Dolatshahi-Pirouz, A.; Foss, M.; Hansen, J. L.; Larsen, A. N.; Zachar, V.; Besenbacher, F.; Yoshida, K. Responses of Fibroblasts and Glial Cells to Nanostructured Platinum Surfaces. *Nanotechnology* **2009**, *20* (38), 385103.
- (39) Dalby, M. J.; Riehle, M. O.; Johnstone, H. J. H.; Affrossman, S.; Curtis, A. S. G. Polymer-Demixed Nanotopography: Control of Fibroblast Spreading and Proliferation. *Tissue Eng.* **2002**, *8* (6), 1099–1108.
- (40) Turner, S.; Kam, L.; Isaacson, M.; Craighead, H. G.; Shain, W.; Turner, J. Cell Attachment on Silicon Nanostructures. *J. Vac. Sci. Technol., B: Microelectron. Process. Phenom.* **1997**, *15* (6), 2848–2854.
- (41) Thevenot, P.; Hu, W.; Tang, L. Surface Chemistry Influences Implant Biocompatibility. *Curr. Top. Med. Chem.* **2008**, *8* (4), 270–280.
- (42) Choe, J. H.; Lee, S. J.; Lee, Y. M.; Rhee, J. M.; Lee, H. B.; Khang, G. Proliferation Rate of Fibroblast Cells on Polyethylene Surfaces with Wettability Gradient. *J. Appl. Polym. Sci.* **2004**, *92* (1), 599–606.
- (43) Kim, S. H.; Ha, H. J.; Ko, Y. K.; Yoon, S. J.; Rhee, J. M.; Kim, M. S.; Lee, H. B.; Khang, G. Correlation of Proliferation, Morphology and Biological Responses of Fibroblasts on LDPE with Different Surface Wettability. *J. Biomater. Sci., Polym. Ed.* **2007**, *18* (5), 609–622.
- (44) Tamada, Y.; Ikada, Y. Fibroblast Growth on Polymer Surfaces and Biosynthesis of Collagen. *J. Biomed. Mater. Res.* **1994**, *28* (7), 783–789.
- (45) Soria, J. M.; Martinez Ramos, C.; Bahamonde, O.; Garcia Cruz, D. M.; Salmeron Sanchez, M.; Garcia Esparza, M. A.; Casas, C.; Guzman, M.; Navarro, X.; Gomez Ribelles, J. L.; Garcia Verdugo, J. M.; Monleon Pradas, M.; Barcia, J. A. Influence of the Substrate's Hydrophilicity on the in Vitro Schwann Cells Viability. *J. Biomed. Mater. Res., Part A* **2007**, *83A* (2), 463–470.
- (46) Gupta, D.; Venugopal, J.; Prabhakaran, M. P.; Dev, V. R. G.; Low, S.; Choon, A. T.; Ramakrishna, S. Aligned and Random Nanofibrous Substrate for the in Vitro Culture of Schwann Cells for Neural Tissue Engineering. *Acta Biomater.* **2009**, *5* (7), 2560–2569.
- (47) Mobasser, S. A.; Terenghi, G.; Downes, S. Schwann Cell Interactions with Polymer Films Are Affected by Groove Geometry and Film Hydrophilicity. *Biomed. Mater.* **2014**, *9* (5), 055004.
- (48) Kalin, M.; Polajnar, M. The Wetting of Steel, DLC Coatings, Ceramics and Polymers with Oils and Water: The Importance and Correlations of Surface Energy, Surface Tension, Contact Angle and Spreading. *Appl. Surf. Sci.* **2014**, *293*, 97–108.
- (49) Ferraris, S.; Cazzola, M.; Peretti, V.; Stella, B.; Spriano, S. Zeta Potential Measurements on Solid Surfaces for in Vitro Biomaterials Testing: Surface Charge, Reactivity Upon Contact With Fluids and Protein Adsorption. *Front. Bioeng. Biotechnol.* **2018**, *6*, 60.
- (50) Kim, B. H.; Yang, S. A.; Kang, S. W.; Choi, G. P.; Cho, S. Y.; Han, J. K.; Lee, G. J.; Lee, M. K.; Seog, H. J.; Kim, I. W.; Bu, S. D. Change of Electrical Properties of $(K_{0.5}Na_{0.5})(Mn_{0.005}Nb_{0.995})O_3$ Thin Films Induced by Gamma-Ray Irradiation. *Curr. Appl. Phys.* **2016**, *16* (5), 539–544.
- (51) Hanawa, T. Metal Ion Release from Metal Implants. *Mater. Sci. Eng., C* **2004**, *24* (6–8), 745–752.
- (52) De Jong, W. H.; Carraway, J. W.; Geertsma, R. E. In Vivo and in Vitro Testing for the Biological Safety Evaluation of Biomaterials and Medical Devices. In *Biocompatibility and Performance of Medical Devices*; Boutrand, J.-P., Ed.; Elsevier Ltd.: Amsterdam, 2020; pp 123–166.
- (53) Ozmen, O.; Ozsoy-Keskinbora, C.; Suvaci, E. Chemical Stability of $KNbO_3$, $NaNbO_3$, and $K_{0.5}Na_{0.5}NbO_3$ in Aqueous Medium. *J. Am. Ceram. Soc.* **2018**, *101*, 1074–1086.

- (54) Puleo, D. A.; Huh, W. W. Acute Toxicity of Metal Ions in Cultures of Osteogenic Cells Derived from Bone Marrow Stromal Cells. *J. Appl. Biomater.* **1995**, *6* (2), 109–116.
- (55) Fraga, C. G. Relevance, Essentiality and Toxicity of Trace Elements in Human Health. *Mol. Aspects Med.* **2005**, *26* (4–5), 235–244.
- (56) Carazeanu Popovici, I.; Lupascu, N. Chemical Durability of Soda-Lime Glass in Aqueous Acid Solutions. *Ovidius Univ. Ann. Chem.* **2012**, *23* (1), 128–132.
- (57) Yang, Y.; Wang, K.; Gu, X.; Leong, K. W. Biophysical Regulation of Cell Behavior - Cross Talk between Substrate Stiffness and Nanotopography. *Engineering* **2017**, *3* (1), 36–54.
- (58) Nemir, S.; West, J. L. Synthetic Materials in the Study of Cell Response to Substrate Rigidity. *Ann. Biomed. Eng.* **2010**, *38* (1), 2–20.
- (59) Flanagan, L. A.; Ju, Y.-E.; Marg, B.; Osterfield, M.; Janmey, P. A. Neurite Branching on Deformable Substrates. *NeuroReport* **2002**, *13* (18), 2411–2415.
- (60) Solon, J.; Levental, I.; Sengupta, K.; Georges, P. C.; Janmey, P. A. Fibroblast Adaptation and Stiffness Matching to Soft Elastic Substrates. *Biophys. J.* **2007**, *93* (12), 4453–4461.
- (61) Kese, K. O.; Li, Z. C.; Bergman, B. Influence of Residual Stress on Elastic Modulus and Hardness of Soda-Lime Glass Measured by Nanoindentation. *J. Mater. Res.* **2004**, *19* (10), 3109–3119.
- (62) Boyd, E. J.; Uttamchandani, D. Measurement of the Anisotropy of Young's Modulus in Single-Crystal Silicon. *J. Microelectromech. Syst.* **2012**, *21* (1), 243–249.
- (63) Egerton, L.; Dillon, D. M. Piezoelectric and Dielectric Properties of Ceramics in the System Potassium-Sodium Niobate. *J. Am. Ceram. Soc.* **1959**, *42* (9), 438–442.
- (64) Brunckova, H.; Medvecký, L.; Hvizdos, P.; Durisin, J. Structural and Nanomechanical Properties of Sol-Gel Prepared (K, Na)NbO₃ Thin Films. *Surf. Interface Anal.* **2015**, *47* (11), 1063–1071.